A fundamental-measure theory for inhomogeneous associating fluids

Yang-Xin Yu[a] and Jianzhong Wu[b]

Department of Chemical and Environmental Engineering, University of California, Riverside, California 92521-0425

The fundamental-measure theory (FMT) of Rosenfeld for hard spheres is extended to inhomogeneous associating fluids on the basis of Wertheim's first-order thermodynamic perturbation theory (TPT1). The excess intrinsic Helmholtz energy, which includes contributions from hard-sphere repulsion and from intermolecular bonding, is represented as a functional of three weighted densities that are related to the geometry of spherical particles. In the absence of association, this theory is the same as the original FMT, and at bulk conditions it reduces to TPT1. In comparison with Monte Carlo simulation results, the extended fundamental-measure theory provides good descriptions of the density profiles and adsorption isotherms of associating hard spheres near a hard wall. Calculated results indicate that the critical temperatures for the vapor–liquid equilibria of associating fluids in hard slit pores are suppressed compared with that for the bulk fluid and the confinement has more significant impact on the liquid side than the vapor side of the coexistence curve. Unlike nonpolar fluids at similar conditions, saturated associating liquids in hard slit pores do not exhibit strong layering near the solid surface. © *2002 American Institute of Physics.* [DOI: 10.1063/1.1463435]

I. INTRODUCTION

Fluids near solid surfaces are commonplace in nature and in engineering, as encountered, for example, in gas storage, oil recovery, heterogeneous catalyst reactions, and removal of various pollutants. Whereas theoretical methods for predicting equilibrium properties of inhomogeneous nonpolar fluids are now well documented,[1] much less understood are the properties of confined associating fluids, including water and asphaltene-containing crude oils in reservoir pores.

Molecular simulations, integral-equation approaches, and density-functional theories are routinely used to investigate the properties of simple (i.e., nonassociating and monomeric) systems at inhomogeneous conditions. However, because of the anisotropic association interactions, molecular simulations are often computationally intensive and analytical theories that give faithful representation of the local fluid structure are yet to be developed.[2] The interplay between chemical association and inhomogeneity makes the phase behavior of confined associating fluids interesting but difficult to predict.[3]

For bulk associating fluids, Wertheim's thermodynamic perturbation theory[4–7] provides a relative simple yet accurate description of thermodynamic properties. With extensions to take into account van der Waals attraction and chain connectivity, Wertheim's theory has been used extensively for describing vapor–liquid equilibria of associating fluids and polymers.[8–11] Applications to inhomogeneous systems have been proposed recently.[12–17] Most current applications of Wertheim's theory are limited to the first-order perturbation that takes into account only the structure of corresponding hard-sphere reference system. While the second-order perturbation theory is more accurate and provides the structure of associating fluid, the computational procedure is more involved. Recently, the second-order Wertheim's theory has been extended to represent the wetting of dimerizing fluids in contact with a hard wall.[18]

Integral-equation theories have been applied to investigate the density profiles of associating fluids near a hard wall.[19,20] These methods are similar to the Henderson–Abraham–Barker (HAB) theory for simple fluids in contact with an impermeable surface where the surface is represented as a distinct component. Solution to the Ornstein–Zernike equation gives pair correlation functions as well as the fluid density profiles and, subsequently, thermodynamic properties. One major limit of this approach is that common closures such as the Percus–Yevick or hypernetted chain approximation are unable to predict phase transitions.

Density-functional theory has been applied extensively to describe interfacial phenomena, including adsorption, wetting, and freezing of fluids at a variety of nonuniform conditions.[21] Like a typical theory for uniform simple fluids, a density-functional theory for inhomogeneous systems is often established following a perturbation approach where hard spheres are used as the reference and attractive interactions are taken into account using mean-field approximations. For instance, Kierlik and Rosinberg[13,14] proposed a perturbation theory for nonuniform hard-sphere-chain fluids based on Wertheim's theory for chain formation and a weighted-density-functional theory for hard-sphere mixtures.[22] Similarly, Segura *et al.*[14,15] presented a density-functional theory that combines Tarazona's receipt for the weighted densities of hard spheres (Mark II)[23,24] with Wertheim's theory for association. Segura's theory agrees well with Monte Carlo simulation for the density profiles of associating hard spheres near a hard wall. It has been success-

fully extended to binary mixtures of associating and neutral hard spheres of equal size.[25] Using the density-functional theory by Segura et al., Pizio et al.[26] calculated the density profiles at the interface of vapor–liquid coexistence for associating fluids in slitlike pores. Also using the density-functional theory by Segura et al., this group investigated density distributions, wetting transitions,[27] and capillary condensations[28] of associating Lennard-Jones fluids in slit-like pores. One drawback of Segura's theory is that it gives poor results near adsorption–desorption transition. Furthermore, extension of Segura's theory to inhomogeneous mixtures containing molecules of different sizes is difficult because the Tarazona weight functions are applicable only to hard spheres of the same size.[21] Following a procedure similar to that used by Segura et al.,[4] Patrykiejew et al. proposed a density-functional approach[29] for nonuniform associating fluids based on the so-called modified Meister–Kroll theory.[30–33] They indicated that this method provides slightly better density profiles compared with that developed by Segura, Chapman, and Shukla.[14]

In this work, we report an extension of the fundamental-measure theory (FMT) of Rosenfeld for hard spheres[34,35] to nonuniform associating fluids. The FMT gives the most accurate descriptions of the structural and thermodynamic properties of inhomogeneous hard-sphere fluids. Unlike most density-functional theories for inhomogeneous systems, FMT is able to predict the structure of homogeneous bulk fluid rather than to use it as an input. It is assumed that the excess intrinsic Helmhotz energy can be expressed in the form of weighted-density approximation with the weight functions taking into account the geometric feature of a spherical particle. The local Helmholtz free energy is derived following the scaled-particle theory. The density-independent weight functions provide the fundamental measure of a spherical particle: two scalar functions representing the averages over particle volume and surface, and a surface vector function representing the density changes across the particle surface. Because these weight functions are independent of density distributions, the weighted densities in FMT are more convenient to calculate than those in most nonlocal density-functional theories. Besides, FMT can be unambiguously extended to mixtures. To extend FMT to associating fluids, we use Wertheim's first-order perturbation theory; but unlike in a typical local-density approximation, the intrinsic Helmholtz energy due to association depends on scalar as well as on vector-weighted densities. In this work the extended FMT has been used to describe the density profiles of associating hard spheres and mixtures of neutral and associating hard spheres near a hard wall or in hard slit pores. Because we are primarily concerned with the properties of the fluid phases, the original formula of FMT is used in this work but inclusion of recent developments of FMT is straightforward.

II. THEORY

A. Model

We consider a binary mixture of neutral and associating hard spheres near a hard wall or confined between two par-

allel hard walls (slit pore). These hard spheres are otherwise identical except some of them have four associating sites placed in the Bol fashion, i.e., the four bonding sites, designated by A, B, C, and D, are placed in tetrahedral symmetry around a spherical core.[36] The pairwise-additive two-body potential is given by[14,25]

$$u(\mathbf{r}_{12},\boldsymbol{\omega}_1,\boldsymbol{\omega}_2)=u_R(r_{12})+\sum_\alpha \sum_\beta u_{\alpha\beta}(\mathbf{r}_{12},\boldsymbol{\omega}_1,\boldsymbol{\omega}_2), \quad (1)$$

where r_{12} is the center-to-center distance between spheres 1 and 2, $\boldsymbol{\omega}_1$ and $\boldsymbol{\omega}_2$ represent the orientations of the two spheres, and the double sum applies over all association sites. The reference potential u_R represents hard-sphere repulsion, given by

$$u_R(r_{12})=\begin{cases} \infty, & r_{12}<(\sigma_1+\sigma_2)/2, \\ 0, & r_{12}>(\sigma_1+\sigma_2)/2, \end{cases} \quad (2)$$

where σ_i designates hard-sphere diameter for component i. In Eq. (1), $u_{\alpha\beta}$ represents the association potential between a bonding site α on a spherical particle and a bonding site β from a different sphere. Following Segura et al.,[14] the association potential is

$$u_{\alpha\beta}(\mathbf{r}_{12},\boldsymbol{\omega}_1,\boldsymbol{\omega}_2)=\begin{cases} -\varepsilon, & r_{12}<r_C,\theta_{\alpha1}<\theta_C,\theta_{\beta2}<\theta_C, \\ 0, & \text{otherwise}, \end{cases} \quad (3)$$

where θ_{Xi} ($X=\alpha,\beta;i=1,2$) is the angle made by the vector from the center of molecule i to the site X and the vector $\mathbf{r}_{12}$. As given in Refs. 14 and 25, only associations between AC, BC, AD, and BD sites are allowed and all the bonding energies are assumed to be identical. The radial limit of association is set to $r_C=0.525(\sigma_1+\sigma_2)/2$ and the angular limit is $\theta_C=27°$.

When the hard spheres are in contact with a single hard wall, the wall potential is

$$\Psi(z)=\begin{cases} \infty, & z\leq 0, \\ 0, & \text{otherwise}, \end{cases} \quad (4)$$

where z is the distance from the center of a hard sphere to the wall. When hard spheres are confined in a slitlike hard pore, the potential due to the confinement is

$$\Psi(z)=\begin{cases} \infty, & z\leq 0 \text{ or } z\geq H, \\ 0, & \text{otherwise}, \end{cases} \quad (5)$$

where H represents the pore width.

B. Density-functional theory

The essential task of a density-functional theory for inhomogeneous fluids is to derive an analytical expression for the grand potential Ω, or equivalently, the intrinsic Helmholtz energy F, as a functional of density distributions. For a binary mixture at given temperature T, total volume V, chemical potential μ_i, and external potential $\Psi_i(\mathbf{r})$ for each component, the grand potential is minimized at equilibrium and the equilibrium density distribution $\rho_i(\mathbf{r})$ satisfies

$$\frac{\delta\Omega}{\delta\rho_i(\mathbf{r})}=0. \quad (6)$$

The grand potential and the intrinsic Helmholtz energy are related by

$$\Omega = F[\rho_1(\mathbf{r}), \rho_2(\mathbf{r})] + \sum_{i=1}^{2} \int d\mathbf{r}\rho_i(\mathbf{r})[\Psi_i(\mathbf{r}) - \mu_i]. \quad (7)$$

Once we have an expression for the intrinsic Helmholtz energy, solution to Eq. (6) gives the equilibrium density profiles and subsequently, relevant thermodynamic properties.

To take into account the nonideality arising from intermolecular interactions, the intrinsic Helmholtz energy is often expressed as contributions from an ideal-gas term and an excess term due to intermolecular interactions

$$F[\rho_1(\mathbf{r}), \rho_2(\mathbf{r})] = F_{id}[\rho_1(\mathbf{r}), \rho_2(\mathbf{r})] + F_{ex}[\rho_1(\mathbf{r}), \rho_2(\mathbf{r})]. \quad (8)$$

The ideal-gas contribution is given by the exact expression

$$F_{id}[\rho_1(\mathbf{r}), \rho_2(\mathbf{r})] = k_B T \sum_{i=1}^{2} \int d\mathbf{r}\rho_i(\mathbf{r})\{\ln(\rho_i(\mathbf{r})\lambda_i^3) - 1\}, \quad (9)$$

where $\lambda_i = h/(2\pi m_i k_B T)^{1/2}$ represents the thermal wavelength with k_B standing for the Boltzmann constant. For most nonideal systems, the excess intrinsic Helmholtz energy can only be evaluated approximately.

As in a typical perturbation approach, we assume that the excess intrinsic Helmholtz energy for a system of inhomogeneous associating hard spheres consists of two terms, the first from the hard-sphere reference system and the second from perturbation

$$F_{ex} = k_B T \int d\mathbf{r}\{\Phi^{hs}[n_\alpha(\mathbf{r})] + \Phi^{assoc}[n_\alpha(\mathbf{r})]\}, \quad (10)$$

where $\Phi[n_\alpha(\mathbf{r})]$ stands for the excess Helmholtz energy density, and the superscripts "hs" and "assoc" denote, respectively, hard-sphere repulsion and association. This decomposition of Helmholtz energy follows the spirit of the interparticle potential as given in Eq. (1).

1. Reference hard-sphere system

The fundamental-measure theory of Rosenfeld provides an expression for the excess intrinsic Helmholtz energy due to hard-sphere interactions. In this theory, the excess intrinsic Helmholtz energy density is represented as a function of six scalar and vector weighted densities $n_\alpha(r)$,[34]

$$n_\alpha(\mathbf{r}) = \sum_i n_{\alpha,i}(\mathbf{r}) = \sum_i \int \rho_i(\mathbf{r}')w_i^{(\alpha)}(\mathbf{r} - \mathbf{r}') d\mathbf{r}', \quad (11)$$

where $\alpha = 0, 1, 2, 3, V1, V2$. Among the six weight functions $w_i^{(\alpha)}(r)$, three of them characterize the geometry of a spherical particle: two scalar functions are related to volume and surface area, and a vector function is related to the gradient across a sphere, i.e.,

$$w_i^{(3)}(r) = \Theta(R_i - r), \quad (12)$$

$$w_i^{(2)}(r) = \delta(R_i - r), \quad (13)$$

$$\mathbf{w}_i^{(V2)}(\mathbf{r}) = (\mathbf{r}/r)\delta(R_i - r). \quad (14)$$

The other three weight functions are proportional to the above geometric functions:

$$n_{0i} = \frac{n_{2i}}{4\pi R_i^2}; \quad n_{1i} = \frac{n_{2i}}{4\pi R_i}; \quad \mathbf{n}_{V1i} = \frac{\mathbf{n}_{V2i}}{4\pi R_i}. \quad (15)$$

In Eqs. (12)–(15), R_i is the hard sphere radius, $\Theta(r)$ is the Heaviside step function, and $\delta(r)$ is the Dirac delta function. For $0 \leq \alpha \leq 3$, the weighted densities $n_\alpha(\mathbf{r})$ have the units of $[n_\alpha] = (\text{volume})^{(\alpha-3)/3}$. The vector-weighted density $\mathbf{n}_{V1}$ has the same units as $n_1(\mathbf{r})$ and $\mathbf{n}_{V2}$ has the same units as $n_2(\mathbf{r})$.

From the scaled-particle differential equation, Rosenfeld derived the following excess Helmholtz energy density for nonuniform hard spheres[37,38]

$$\Phi^{hs}\{n_\alpha(\mathbf{r})\} = \Phi_1^{hs} + \Phi_2^{hs} + \Phi_3^{hs}, \quad (16)$$

where

$$\Phi_1^{hs} = -n_0 \ln(1 - n_3), \quad (17)$$

$$\Phi_2^{hs} = \frac{n_1 n_2 - \mathbf{n}_{V1} \cdot \mathbf{n}_{V2}}{(1 - n_3)}, \quad (18)$$

$$\Phi_3^{hs} = \frac{\frac{1}{3}n_2^3 - n_2 \mathbf{n}_{V2} \cdot \mathbf{n}_{V2}}{8\pi(1 - n_3)^2}. \quad (19)$$

In Eqs. (18) and (19), $\mathbf{n}_{V1}$ and $\mathbf{n}_{V2}$ are vectors, and $\mathbf{n}_{V1} \cdot \mathbf{n}_{V2}$ is a dot product. In the limit of a homogeneous fluid, the two vector-weighted densities $\mathbf{n}_{V1}$ and $\mathbf{n}_{V2}$ vanish, and the Helmholtz energy becomes identical to that derived from the Percus–Yevick theory.

Equation (17) is exact in the limit of one-dimensional hard-rod fluid.[39] The first and second terms on the right-hand side of Eq. (16) give a reasonable approximation for the Helmholtz energy of hard disks. Corrections to the third term on the right side of Eq. (16) have been proposed to improve the performance of the fundamental-measure theory in reduced dimensionality.[39,40] In this work we use the original expression because the focus here is on the equilibrium properties of nonuniform fluids, for which the corrections have only marginal effects.

In the limit of a uniform fluid, the density distribution for each component becomes the corresponding bulk density, $\rho_i(\mathbf{r}) \equiv \rho_{b,i}$, and the scalar-weighted densities coincide with the variables of the scaled-particle theory for bulk hard spheres

$$n_{0i} = \rho_{b,i}, \quad n_{1i} = R_i \rho_{b,i}, \quad n_{2i} = 4\pi R_i^2 \rho_{b,i},$$

$$n_{3i} = 4\pi R_i^3 \rho_{b,i}/3. \quad (20)$$

2. Perturbation

For a bulk associating fluid, the Helmholtz energy density due to associations is given by

$$\Phi^{assoc,b} = \sum_i M_i \rho_{b,i} \left(\ln \chi_\alpha^{b,i} - \frac{\chi_\alpha^{b,i}}{2} + \frac{1}{2} \right), \quad (21)$$

where M_i is the number of association sites per molecule of species i, $\chi_\alpha^{b,i}$ is the fraction of molecules of component i not bonded at site A. In Eq. (21), $\chi_\alpha^{b,i}$ is calculated from

$$\chi_\alpha^{b,i} = \frac{1}{1 + \Sigma_j \rho_{b,j} \Sigma_\alpha \chi_\alpha^{b,j} \Delta^{i,j}}, \tag{22}$$

where $\Delta^{i,j} = 4\pi K g_{ij}^{\mathrm{hs},b}(\sigma_{ij}) f_{\alpha\beta}$, K is a constant reflecting the volume available for bonding of the two sites on molecules 1 and 2, $f_{\alpha\beta} = \exp(\varepsilon/k_B T) - 1$ represents the Mayer function, and $g_{ij}^{\mathrm{hs},b}(\sigma_{ij})$ is contact value of the hard-sphere pair correlation function:

$$g_{ij}^{\mathrm{hs},b}(\sigma_{ij}) = \frac{1}{1-\xi_3} + \frac{3\sigma_i\sigma_j}{\sigma_i+\sigma_j}\frac{\xi_2}{(1-\xi_3)^2}$$
$$+ 2\left(\frac{\sigma_i\sigma_j}{\sigma_i+\sigma_j}\right)^2 \frac{\xi_2^2}{(1-\xi_3)^3}, \tag{23}$$

with $\xi_m = (\pi/6)\Sigma_{i=1}^2 \rho_i \sigma_i^m$, $m = 0,1,2,3$, and $\sigma_{ij} = (\sigma_i + \sigma_j)/2$. Following Segura et al.,[14,25] we use $K = 1.4849 \times 10^{-4} \sigma^3$ in the following calculations.

The excess Helmholtz energy due to association is taken into account using the weighted-density approximation. To extend Eq. (21) to inhomogeneous systems, intuitively we may replace ξ_3, ξ_2 and $\rho_{b,i}$ in Eqs. (21)–(23) with, respectively, n_3, $\frac{1}{6}n_2$ and n_{0i} as suggested by Eq. (20). This approach includes only the scalar-weighted densities in calculating the Helmholtz energy. In order to take into account the vector-weighted densities, we introduce two proportional factors $\zeta_i = 1 - \mathbf{n}_{V2i}\cdot\mathbf{n}_{V2i}/n_{2i}^2$ and $\zeta = 1 - \mathbf{n}_{V2}\cdot\mathbf{n}_{V2}/n_2^2$, to "correct" the weighted densities n_{0i}, n_2, and n_2^2. In other words, we replace ξ_3, ξ_2, ξ_2^2, and $\rho_{b,i}$ in Eqs. (21)–(23) with n_3, $\frac{1}{6}n_2\zeta$, $\frac{1}{36}n_2^2\zeta$, and $n_{0i}\zeta_i$, respectively. In this case, the Helmholtz energy density of association becomes

$$\Phi^{\mathrm{assoc}}(n_\alpha) = \sum_{i=1}^2 n_{0i}\zeta_i M_i \left[\ln\chi_A^{(i)}(\mathbf{r}) - \frac{\chi_A^{(i)}(\mathbf{r})}{2} + \frac{1}{2}\right], \tag{24}$$

where $\chi_A^{(i)}(\mathbf{r})$ is the fraction of molecules i at position $\mathbf{r}$ not bonded at site A, and it is obtained from

$$\chi_A^{(i)}(\mathbf{r}) = \frac{1}{1 + \Sigma_j n_{0j}\zeta_j \Sigma_\alpha \chi_\alpha^{(j)}(\mathbf{r})\Delta^{ij}(\mathbf{r})}, \tag{25}$$

where

$$\Delta^{ij}(\mathbf{r}) = 4\pi K g_{ij}^{\mathrm{hs}}(\sigma_{ij}, n_\alpha) f_{\alpha\beta}, \tag{26}$$

$$g_{ij}^{\mathrm{hs}}(\sigma_{ij}, n_\alpha) = \frac{1}{1-n_3} + \frac{\sigma_i\sigma_j}{\sigma_i+\sigma_j}\frac{n_2\zeta}{2(1-n_3)^2}$$
$$+ \left(\frac{\sigma_i\sigma_j}{\sigma_i+\sigma_j}\right)^2 \frac{n_2^2\zeta}{18(1-n_3)^3}. \tag{27}$$

Once we have an expression for the intrinsic Helmholtz energy, minimization of the grand potential with respect to the density distributions [Eq. (6)] leads to the Euler–Lagrange equation

$$\rho_i(\mathbf{r}) = \lambda_i^{-3} \exp\{c_i^{(1)}[\mathbf{r}, \rho_1(\mathbf{r}), \rho_2(\mathbf{r})]$$
$$+ [\mu_i - \psi_i(\mathbf{r})]/(k_B T)\}, \tag{28}$$

where $c_i^{(1)}[\mathbf{r}, \rho_1(\mathbf{r}), \rho_2(\mathbf{r})]$ is the one-particle direct correlation function, obtained from

$$c_i^{(1)}[\mathbf{r}, \rho_1(\mathbf{r}), \rho_2(\mathbf{r})] = -\frac{1}{k_B T}\frac{\delta F_{\mathrm{ex}}[\rho_1(\mathbf{r}), \rho_2(\mathbf{r})]}{\delta\rho_i(\mathbf{r})}$$
$$= -\int dr' \sum_\alpha \frac{\partial(\Phi^{\mathrm{hs}} + \Phi^{\mathrm{assoc}})}{\partial n_\alpha}$$
$$\times w_i^{(\alpha)}(r - r'). \tag{29}$$

At equilibrium, the chemical potentials of all species remain constant. When the confined fluid is in equilibrium with a bulk phase, the chemical potential can be calculated from

$$\mu_i = k_B T \ln(\rho_{b,i}\lambda_i^3) + \mu_i^{\mathrm{ex,hs}} + \mu_i^{\mathrm{ex,assoc}}, \tag{30}$$

where the first term on the right-hand side comes from the idea-gas reference state, the hard-sphere term $\mu_i^{\mathrm{ex,hs}}$ is from the scaled-particle theory,[41] and the association chemical potential is calculated from Wertheim's thermodynamic perturbation theory.[4–10]

III. RESULTS AND DISCUSSION

We apply the Picard-type iterative method to solve the Euler–Lagrange equation [Eq. (28)]. For hard spheres near a hard wall or within slit pores, the density distributions vary only in one direction. To avoid divergence, it is necessary to mix the new and old density profiles in certain proportions during the iteration process, i.e.,

$$\rho_{\mathrm{in}}^{(i+1)}(z) = \rho_{\mathrm{out}}^{(i)}(z)f + \rho_{\mathrm{in}}^{(i)}(1-f). \tag{31}$$

The mixing parameter f varies from 0.01 at high densities ($\rho_b^* \geq 0.9$) to close to unity at low densities. The exact value is obtained by trial and error method.

The weighted densities and the integrals in Eq. (29) are evaluated by a trapezoidal rule with a mesh width equal to 0.01σ for a satisfactory numerical accuracy. The iterations terminate when the maximum difference between two subsequent density profiles is smaller than 10^{-7}. Once the density profiles are obtained, the fractions of molecules i at position z not bonded at site α are calculated from[42]

$$\chi_\alpha^{(i)}(z) = \left[1 + 4\pi K g^{\mathrm{hs}}(\sigma_i, \rho_{b,i}) \right.$$
$$\left. \times \int_{-1+z}^{1+z} \chi_\alpha^{(i)}(z')\rho_i(z')\, dz' \right]^{-1}, \tag{32}$$

where $g^{\mathrm{hs}}(\sigma_i, \rho_{b,i})$ is the contact value of the hard-sphere pair correlation function at the bulk density $\rho_{b,i}$. With the assumptions that all four sites are equivalent regardless of the distance from the hard wall, the fraction of monomers can be approximated by

$$\chi_0(z) = \chi_\alpha^4(z). \tag{33}$$

The surface excess for component i at the hard wall is related to the density profile by

$$\Gamma_i \sigma_i^2 = \int_0^\infty [\rho_i(z)\sigma_i^3 - \rho_{b,i}\sigma_i^3]\, dz, \tag{34}$$

where $\rho_i(z)\sigma_i^3$ is the local reduced number density and $\rho_{b,i}(z)\sigma_i^3$ is the reduced number density in the bulk.
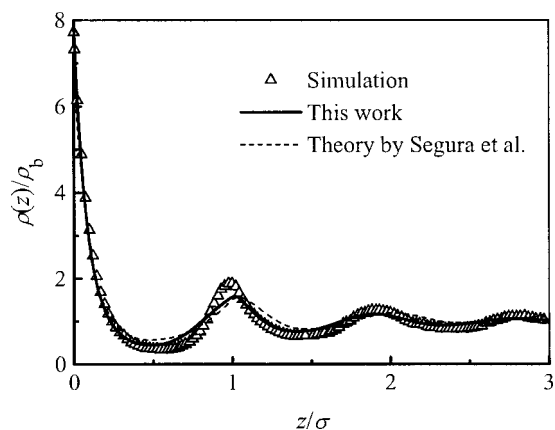
FIG. 1. Density profiles of associating hard spheres near a hard wall from the theory by Segura *et al.* (Ref. 14) (dash line), from the extended FMT (solid line), and from simulation (open triangles). Here $1/T^*=5$, $\rho_b^*=0.9036$.

A. An associating fluid near a hard wall

The following comparison between the density-functional theory and simulation results is based on the same set of parameters for intermolecular potentials and bulk densities. No adjustable parameter is used. In all these calculations, the particles have the same diameter σ. The definition of the reduced temperature and reduced density are given by, respectively, $T^*=k_B T/\varepsilon$ and $\rho^*=\rho\sigma^3$, where ε is the site bonding energy.

Figure 1 shows the density profile of associating hard spheres at temperature $1/T^*=5$ and bulk density ρ_b^*
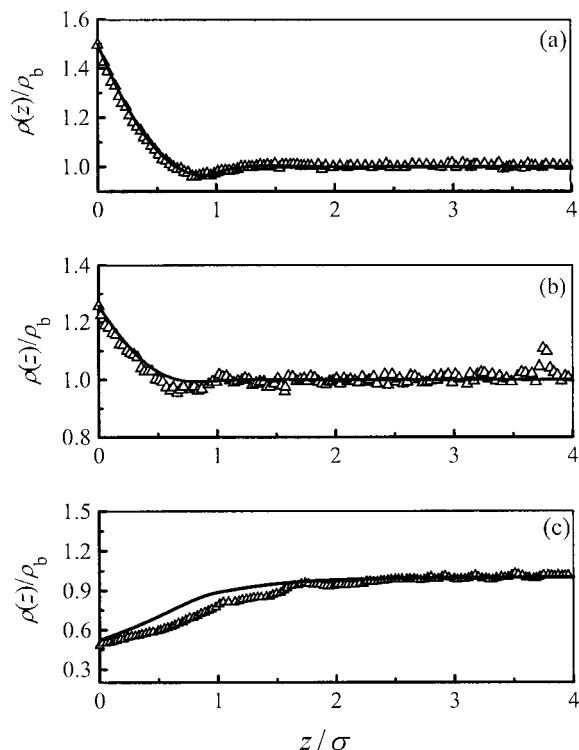

FIG. 2. Density profiles of associating hard spheres against a hard wall (a) $\rho_b^*=0.1977$, $1/T^*=3$; (b) $\rho_b^*=0.1994$, $1/T^*=5$; and (c) $\rho_b^*=0.2112$, $1/T^*=7$. The open triangles represent the simulation results (Ref. 14), the solid lines represent the calculated results from the extended FMT.
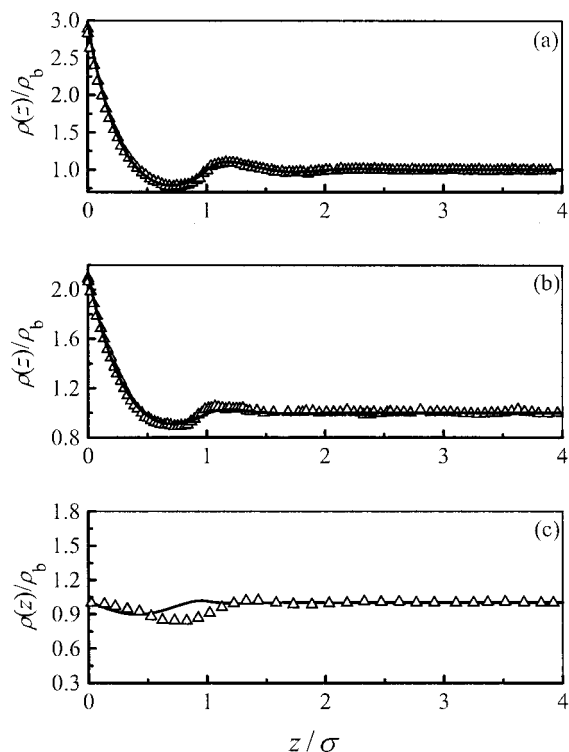

FIG. 3. Same as Fig. 2 but (a) $\rho_b^*=0.4874$, $1/T^*=3$; (b) $\rho_b^*=0.4914$, $1/T^*=5$; and (c) $\rho_b^*=0.5239$, $1/T^*=7$.

$=0.9036$ near a hard wall predicted from the extended fundamental-measure theory. Also shown in Fig. 1 are the corresponding results from Monte Carlo simulation and from the density-functional theory proposed by Segura *et al.*[14] Figure 1 does not include the results from the inhomogeneous version of Wertheim's theory because it gives much too high peaks in the density profiles. In this example, both density-functional theories agree reasonably well with Monte Carlo simulation results; however, the theory present here has the advantage of numerical simplicity because the weight functions are independent of density.

Figures 2–5 compare the density distributions of associating hard spheres near a hard wall predicted from the extended fundamental-measure theory with those from molecular simulations at four average reduced densities: $\rho^*=0.2$, 0.5, 0.75, and 0.942, and for each densities, three reduced bonding energies: $\varepsilon/k_B T=3$, 5, and 7. In most cases the present theory provides satisfactory density profiles except near the freezing point, where it slightly overestimates the contact values. Similar discrepancy has been observed when FMT is applied to hard-sphere fluid near a hard wall.

Figure 2 indicates that at a low overall average density, the associating hard spheres are adsorbed to a hard wall when the bonding is weak but become depleted from the wall when the bonding energy is sufficiently high. Adsorption at small association energy is due to the excluded volume effect as occurred in a neutral hard-sphere system. At high association energy, the surface effects extended far from the wall, which suggests a long-range solvation force. In this case, the present theory slightly overestimates the density distributions in the depletion zone.
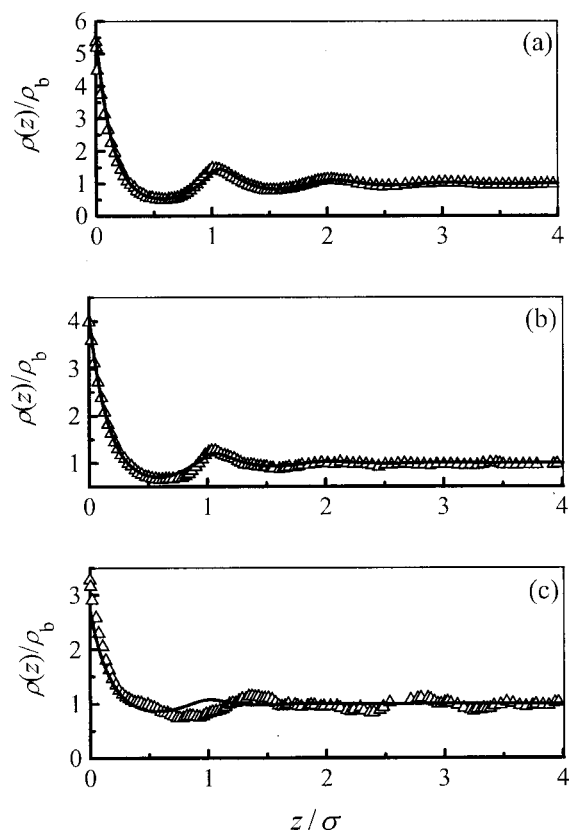
FIG. 4. Same as Fig. 2 for (a) $\rho_b^* = 0.7191$, $1/T^* = 3$; (b) $\rho_b^* = 0.7257$, $1/T^* = 5$; and (c) $\rho_b^* = 0.7366$, $1/T^* = 7$.

FIG. 5. Same as Fig. 2 for (a) $\rho_b^* = 0.9158$, $1/T^* = 3$; (b) $\rho_b^* = 0.9036$, $1/T^* = 5$; and (c) $\rho_b^* = 0.9085$, $1/T^* = 7$.

As density increases, the density profiles shift toward the wall, as shown in Figs. 3 and 4. It is interesting to note that in Fig. 3(c), where the overall reduced density equal to 0.5 and $1/T^* = 7$, associating hard spheres are slightly desorbed from the hard wall and, due to the cancellation of association and excluded volume effects, the density distribution appears uniform. The simulation data in Fig. 3(c) are from Patrykie-jew *et al.*[27]

Figure 5 presents the density distributions of associating hard spheres when the bulk density is close to the hard-sphere freezing point. While the extended FMT theory predicts accurate peak positions, it gives slightly too high contact values. The discrepancy probably arises from the approximations used in the FMT.

The local fraction of unbonded associating hard spheres is calculated from Eq. (32). Figure 6 gives the monomer fraction $\chi_0(z)$ as a function of the distance from the hard wall for the systems as given in Fig. 2. Monomer fraction falls away from the wall because the presence of the wall blocks some bonding sites. While in general the theory agrees well with simulation results, Fig. 6 indicates that the discrepancy increases with the association energy. All the monomer profiles exhibit a change in slope at $z = \sigma$. This cusp is related to the integral in Eq. (32) and the approximation that bonding occurs only at hard-sphere contact.[14] Specifically, if a molecule sits at $z < \sigma$, its association with a second molecule on the wall side is restricted by the excluded volume effect; while far from the wall ($z > \sigma$), the
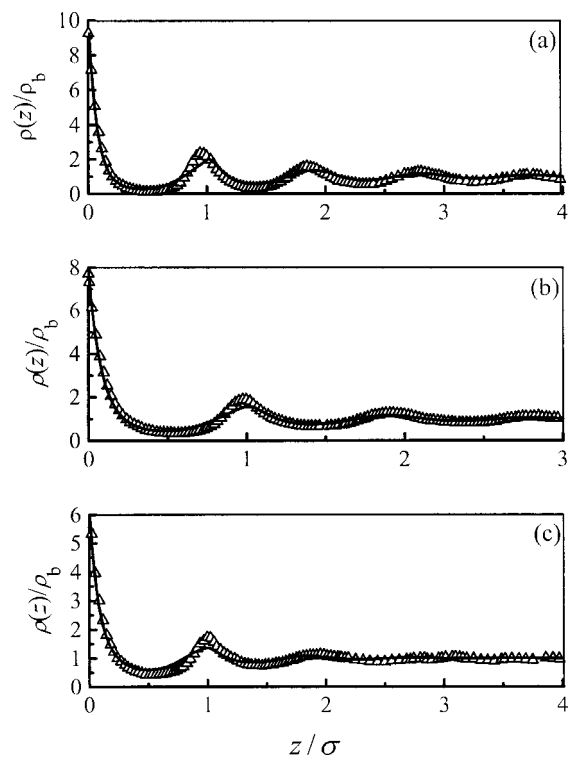
wall has little effect on intermolecular bonding and $\chi_0(z)$ is almost constant.

Figure 7 shows calculated and simulated adsorption isotherms of the four-site associating hard-sphere fluid near a hard wall at $1/T^* = 0$, 5, and 7. All three adsorption isotherms correspond to supercritical conditions (the corresponding equation of state for bulk fluids gives the critical temperature $\varepsilon/k_B T_c = 1/T_c^* = 7.76$). At a low bonding energy, the surface excess increases monotonically with the bulk density. However, when the bonding energy is sufficiently high, the surface excess first decreases with the bulk density
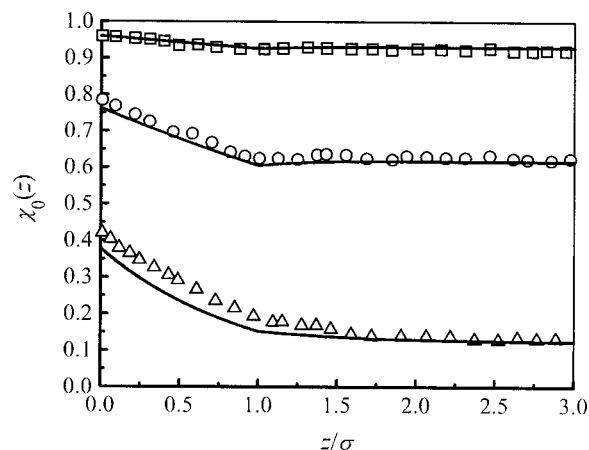

FIG. 6. Local monomer fraction for the associating hard-sphere fluid near a hard wall. The symbols represent simulation data (Ref. 14) and solid lines represent the extended FMT results. The curves, from top to bottom, are for $\rho_b^* = 0.1977$, $1/T^* = 3$ (squares); $\rho_b^* = 0.1994$, $1/T^* = 5$ (circles); and $\rho_b^* = 0.2112$, $1/T^* = 7$ (triangles).
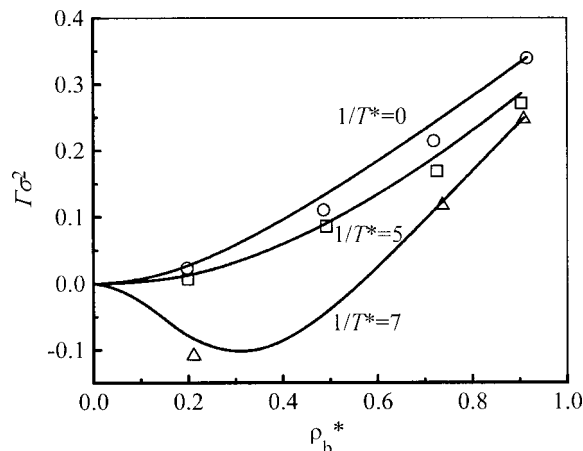
FIG. 7. Adsorption isotherms of the four-site associating hard sphere fluid near a hard wall. The symbols represent the simulation data (Ref. 14) and solid lines represent the results of the extended FMT. The curves, from top to bottom, are for $1/T^*=0$ (circles), $1/T^*=5$ (squares), and $1/T^*=7$ (triangles).
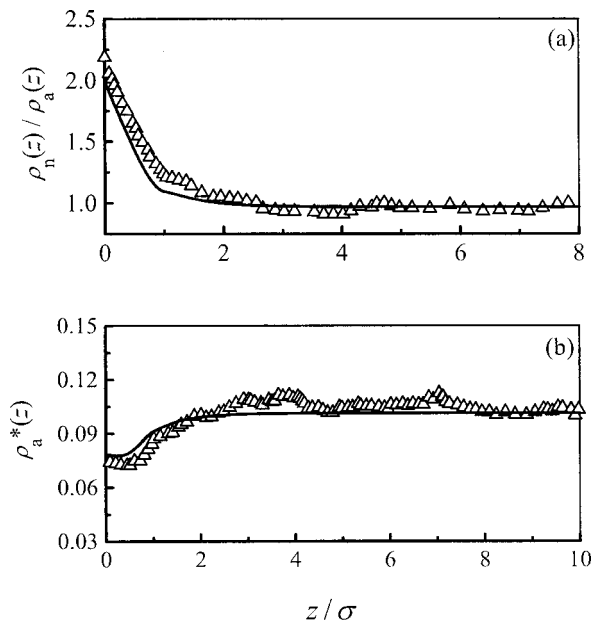

FIG. 8. A binary associating fluid mixture ($\rho_b^*=0.1996$, $\rho_{b,a}^*=0.1014$, $1/T^*=7$) near a hard wall: (a) the ratio of hard spheres to associating spheres versus distance from the wall; (b) the reduced density of associating spheres versus distance from the wall. The symbols represent Monte Carlo simulation results (Ref. 25) and the solid line represents the result of the extended FMT.

[due to the depletion effect as shown in Fig. 2(c)], exhibits a minimum, and finally rises as the density is further increased. The desorption to adsorption transition of associating hard spheres can be explained by the competition between excluded-volume and bonding: the excluded volume favors accumulation of hard spheres near the wall but because the wall is neutral, bonding between hard spheres are restricted close to the wall. At low densities and high bonding energies, the association effect prevails and the density profile shows depletion, whereas at conditions of high density and low association energy, in contrast, the density profile is dominated by the excluded-volume effect, leading to adsorption. The adsorption isotherms predicted by the density-functional theory are in good agreement with results from molecular simulation at both high and low association energies.

B. Binary mixtures of associating fluids near a hard wall

We also investigated the density profiles of binary mixtures of neutral and associating hard spheres near a hard wall. For comparison with simulation results, all hard spheres considered here have the same size. Figures 8–10 show the ratios of hard-sphere density to associating sphere density, $\rho_n(z)/\rho_a(z)$, and the normalized density profiles of associating spheres, $\rho_a(z)/\rho_{b,a}$, as functions of the distance from the wall at several bulk densities and temperatures. Here $\rho_a(z)$ represents the density distribution of four-site associating hard spheres, $\rho_n(z)$ is the density distribution of neutral hard spheres, and $\rho_{b,a}$ is the bulk density of associating hard spheres.

Figure 8 compares the density profiles calculated from the extended fundamental-measure theory with those from Monte Carlo simulation results[25] at $\rho_b^*=0.1996$, $\rho_{b,a}^*=0.1014$, $1/T^*=7$. Both theory and simulation show a depletion of associating particles near the hard wall. As discussed earlier, that depletion is induced by the reduction of the accessibility of the bonding sites. Close to the hard wall the density of associating spheres falls initially and

then increases with the distance. Figures 8(a) and 8(b) indicate while the extended fundamental-measure theory catches the essential details, it overestimates slightly the local density near the wall.

Figure 9 gives the density profiles at the same reduced temperature as that given in Fig. 8 but at higher reduced
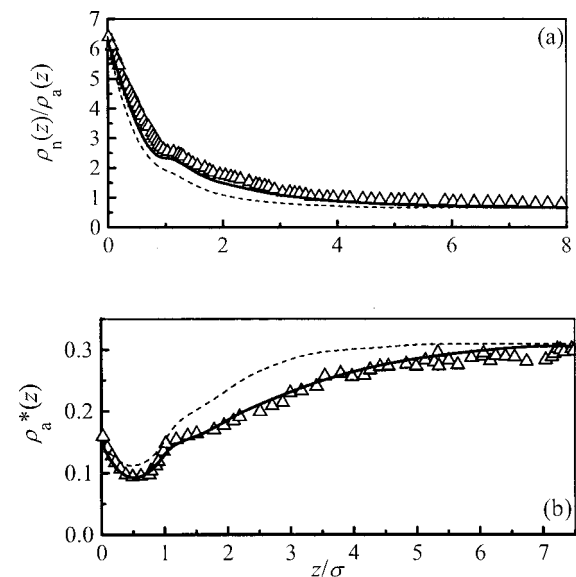

FIG. 9. A binary associating fluid mixture ($\rho_b^*=0.5134$, $\rho_{b,a}^*=0.3089$, $1/T^*=7$) near a hard wall: (a) ratio of hard spheres to associating spheres versus distance from the wall; (b) reduced density of associating spheres versus distance from the wall. The symbols represent Monte Carlo simulation results (Ref. 25), the dashed line represents the result from the theory by Segura et al. (Ref. 25), and the solid line represents the result of the extended FMT.
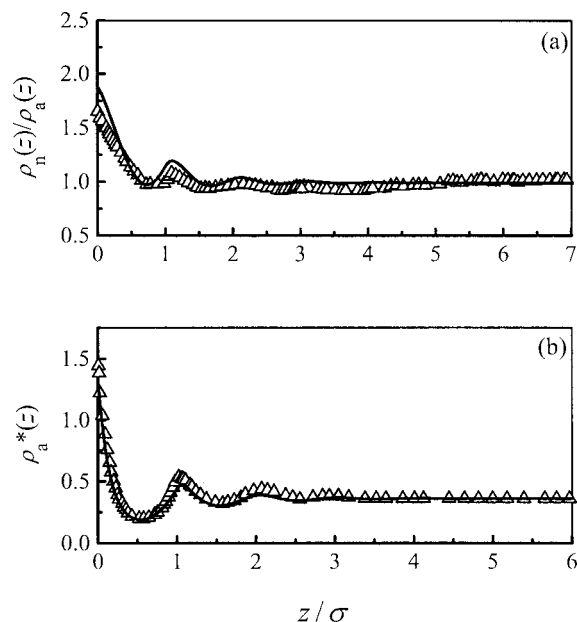
FIG. 10. Same as Fig. 8 for $\rho_b^* = 0.7173$, $\rho_{b,a}^* = 0.3604$, and $1/T^* = 5$.
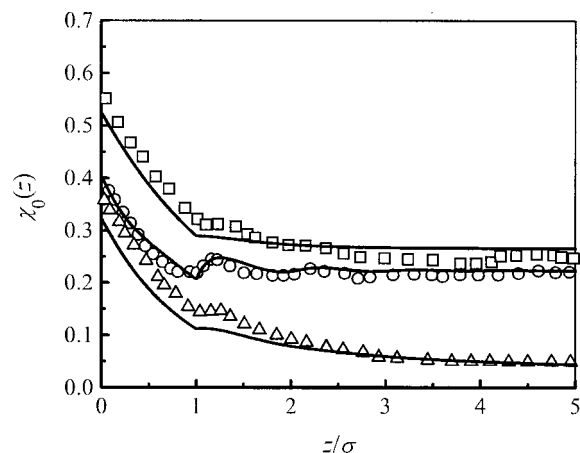

FIG. 11. Fraction of unbonded associating hard spheres near a hard wall in binary mixtures. The symbols represent the simulation data (Ref. 25) and the lines represent the results of the extended FMT. The curves, from top to bottom, are for $\rho_b^* = 0.1996$, $\rho_{b,a}^* = 0.1014$, $1/T^* = 7$ (squares); $\rho_b^* = 0.7173$, $\rho_{b,a}^* = 0.3604$, $1/T^* = 5$ (circles); and $\rho_b^* = 0.5134$, $\rho_{b,a}^* = 0.3089$, $1/T^* = 7$ (triangles).

densities ($\rho_b^* = 0.5134$, $\rho_{b,a}^* = 0.3089$, $1/T^* = 7$). Also shown in this figure are simulation and calculated results from Segura *et al.*[25] Figure 9 shows that Segura's theory underestimates the depletion effect and, consequently, the ratio of local densities for hard spheres and associating spheres. Both theoretical methods correctly predict the little kink around $z = 1\sigma$. In Fig. 9(b), the trough near the wall is enhanced in comparison with that in Fig. 8(b).

Figure 10 presents the ratio of the local densities of hard spheres and associating spheres as well as the density distribution of associating spheres near a hard wall at $\rho_b^* = 0.7173$, $\rho_{b,a}^* = 0.3604$, and $1/T^* = 5$. Both density and temperature here are higher than those in Fig. 9. In this case, the density profiles are dominated by the excluded-volume effect so that even associating spheres show adsorption to the wall. It is interesting to note that the ratio of local densities of hard spheres and the associating spheres shows a maximum at an intermediate density [Figs. 8(a), 9(a), and 10(a)]. Figures 8–10 indicate that the extended fundamental-measure theory predicts the local compositions and density profiles in favorable agreement with those from molecular simulations.

Figure 11 shows the fraction of unbonded associating hard spheres as a function of the distance from the hard wall for the three binary mixtures considered in Figs. 8–10. The extended fundamental measure theory works best for the case corresponding to $\rho_b^* = 0.7173$, $\rho_{b,a}^* = 0.3604$, and $1/T^* = 5$ while it underestimates the monomer profile for the other two cases. In all cases the local density of monomers exhibits a change in slope at $z = \sigma$.

C. Capillary condensation in a slitlike pore

We now apply the extended fundamental-measure theory to investigate the phase behavior of the associating hard spheres in slitlike hard pores. For the vapor–liquid equilibrium of confined fluids, the coexistence point is found by the equality of the grand canonical potentials Ω for the two dis-

tinct density profiles at a fixed temperature T and chemical potential μ. In other words, at vapor–liquid equilibrium, two sets of density distributions can be found that give the same minimum grand potential. The average density in the pore ρ_{av} is calculated from

$$\rho_{av} = \int_0^H \rho(z)\, dz / H. \tag{35}$$

When the pore width is infinite, the average densities in the pore correspond to those for saturated bulk vapor and liquid phase, i.e., $\rho_{av} = \rho_b$. In this case, the requirement of equal grand potential between vapor and liquid phases at constant temperature, volume, and chemical potential is equivalent to that of equal in pressure because for a bulk fluid, the grand potential is $\Omega = -PV$.

Figure 12 shows the vapor–liquid coexistence curves for the bulk and for the confined associating hard spheres at the pore width equal to $H = 10\sigma$ and 20σ. As for confined nonpolar fluids, the coexistence curves in the slit pore are narrowed and the critical temperatures are depressed relative to that for the bulk case. The density for the liquid side of the coexistence curve is considerably lower than that for the bulk because the depletion of associating spheres from the hard walls leads to a low value of the average density. The insert plot in Fig. 12 magnifies the vapor side of the coexistence curves. The condensation density of confined associating hard spheres within a hard slit pore could be higher or lower than that corresponding to the bulk phase, depending on the system temperature. The confinement causes a small decrease in the critical density. The entire phase diagram for associating fluid is shifted toward lower temperatures and lower densities in comparison with the corresponding bulk phase diagram. Simulation results are not presented in Fig. 12 because we are not aware of any data for the vapor–liquid coexistence of confined associating fluids.
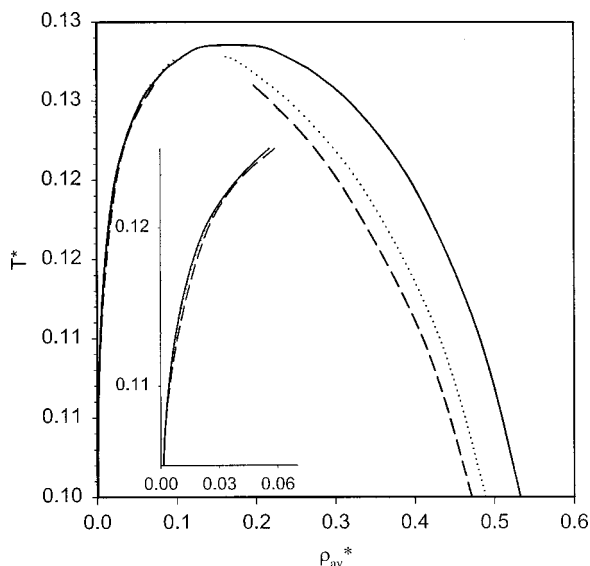
FIG. 12. Phase diagrams for a four-site associating hard-sphere fluid in bulk (solid lines) and in slitlike pores of different width ($H=10\sigma$, dashed lines and 20σ, dotted lines).

Figure 13 shows the density profiles of the saturated vapor and liquid phases at two pore widths given in Fig. 12. Here the reduced density of the liquid phase is about 0.3, close to that given in Fig. 2(c). These relatively smooth den-

sity profiles are dramatically different from those for confined nonpolar fluids where strong oscillation in density distributions has been observed.

IV. CONCLUSIONS

A new density-functional theory is presented to describe the behavior of associating hard spheres near a hard wall or within hard slitlike pores based on the fundamental-measure theory in conjunction with Wertheim's thermodynamic perturbation theory. Extensive comparison with Monte Carlo simulation results for the density profiles, the fraction of monomers, and adsorption isotherms of associating hard-sphere fluids near a hard wall indicates that the current theory is fairly accurate except near freezing where it slightly overestimates the contact values. As observed in Monte Carlo simulations, the calculations presented here confirm that association has significant effect on the adsorption/desorption of molecules near a hard-sphere surface. The large depletion zone of associating hard spheres near a hard wall suggests that the solvation force in an associating fluid could be long ranged.

We also calculated the vapor–liquid coexistences of confined associating hard spheres in hard slit pores. In general, the confinement depresses the two-phase region, as observed in inhomogeneous nonpolar fluids. The confinement has a larger effect on the liquid side of the coexistence line than that on the vapor side, probably due to the depletion of associating molecules from the hard surface. On the vapor side, the condensation density of confined associating hard spheres within a hard slit pore could be higher or lower than that corresponding to the bulk phase, depending on temperature. We found that the density profiles of coexisting vapor and liquid phases are very different from those for confined nonpolar systems.

For one-component associating hard spheres at low densities, this new density-functional theory has similar accuracy compared with the theory by Segura et al.;[14,25] but at high densities and for mixtures, it gives better results. Because the weight functions used here are independent of density, the present density-functional theory is computationally more efficient than other nonlocal weighted density methods. Moreover, the present theory can be directly applied to mixtures of associating fluids, including those with different sizes and those containing chain molecules.

[1] L. D. Gelb, K. E. Gubbins, R. Radhakrishnan, and M. Sliwinska-Bartkowiak, Rep. Prog. Phys. **62**, 1573 (1999).
[2] M. Borowko, *Computational Methods in Surface and Colloid Science* (Marcel Dekker, New York, 2000).
[3] A. Kovalenko, A. Trokhymchuk, O. Pizio, and D. Henderson, Mol. Phys. **89**, 1765 (1996).
[4] M. S. Wertheim, J. Stat. Phys. **35**, 19,35 (1984).
[5] M. S. Wertheim, J. Stat. Phys. **42**, 459,477 (1985).
[6] M. S. Wertheim, J. Chem. Phys. **85**, 2929 (1986).
[7] M. S. Wertheim, J. Chem. Phys. **88**, 1145 (1988).
[8] W. G. Chapman, K. E. Gubbins, G. Jackson, and M. Radosz, Fluid Phase Equilib. **52**, 31 (1989).
[9] W. G. Chapman, K. E. Gubbins, G. Jackson, and M. Radosz, Ind. Eng. Chem. Res. **29**, 1709 (1990).
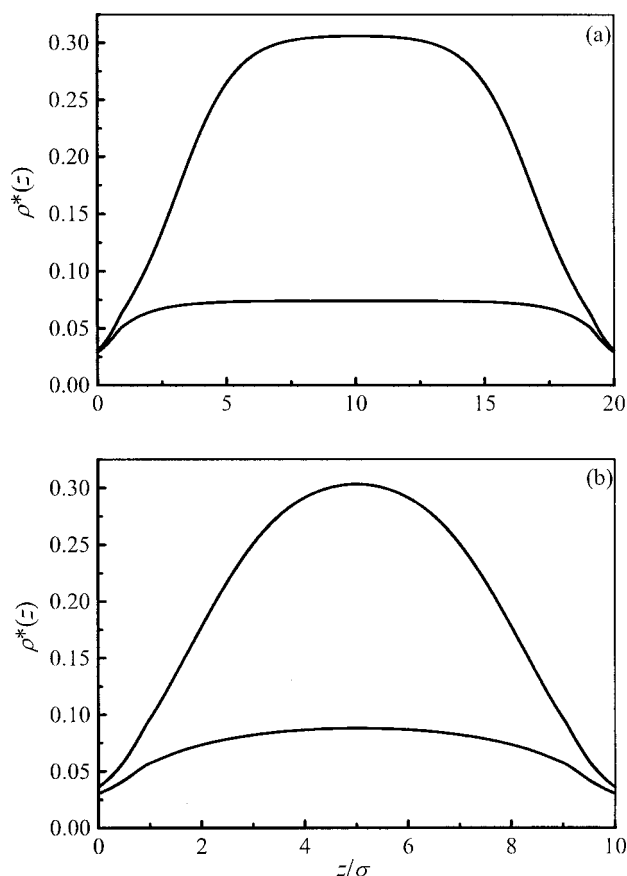
FIG. 13. Density profiles of the coexisting vaporlike and liquidlike phases for the four-site associating hard-sphere fluid in hard slit pores at $1/T^*=0.126$ with pore width (a) $H=20\sigma$ and (b) $H=10\sigma$.

J. Chem. Phys., Vol. 116, No. 16, 22 April 2002

Theory of inhomogeneous associated fluids 7103

[10] A. Galindo, P. J. Whitehead, G. Jackson, and A. N. Burgess, J. Chem. Phys. **100**, 6781 (1998).

[11] Y.-X. Yu, J.-F. Lu, J.-S. Tong, and Y.-G. Li, Fluid Phase Equilib. **102**, 159 (1994).

[12] E. Kierlik and M. L. Rosinberg, J. Chem. Phys. **97**, 9222 (1992).

[13] E. Kierlik and M. L. Rosinberg, J. Chem. Phys. **100**, 1716 (1994).

[14] C. J. Segura, W. G. Chapman, and K. P. Shukla, Mol. Phys. **90**, 759 (1997).

[15] C. J. Segura, E. V. Vakarin, W. G. Chapman, and M. F. Holovko, J. Chem. Phys. **108**, 4837 (1998).

[16] M. F. Holovko and E. Vakarin, Mol. Phys. **85**, 1057 (1995).

[17] O. Pizio, D. Henderson, and S. Sokolowski, J. Phys. Chem. **99**, 2408 (1995); Y. Duda, D. Henderson, A. Trokhymchuk, and D. Wasan, J. Chem. Phys. **103**, 7495 (1999).

[18] A. Trokhymchuk, O. Pizio, D. Henderson, and S. Sokolowski, Chem. Phys. Lett. **262**, 33 (1996).

[19] M. F. Holovko and E. V. Vakarin, Mol. Phys. **84**, 1057 (1994).

[20] M. F. Holovko and E. V. Vakarin, Mol. Phys. **87**, 1375 (1996).

[21] R. Evans, *Fundamentals of Inhomogeneous Fluids*, edited by D. Henderson (Dekker, New York, 1992).

[22] E. Kierlik and M. L. Rosinberg, Phys. Rev. A **42**, 3382 (1990).

[23] P. Tarazona, Phys. Rev. A **31**, 2672 (1985).

[24] P. Tarazona, U. M. B. Marconi, and R. Evans, Mol. Phys. **60**, 573 (1987).

[25] C. J. Segura, J. Zhang, and W. G. Chapman, Mol. Phys. **99**, 1 (2001).

[26] O. Pizio, A. Patrykiejew, and S. Sokolowski, J. Chem. Phys. **113**, 10761 (2000).

[27] A. Patrykiejew, S. Sokolowski, and D. Henderson, Mol. Phys. **97**, 919 (1999).

[28] K. Stepniak, A. Patrykiejew, Z. Sokolowski, and S. Sokolowski, J. Colloid Interface Sci. **214**, 91 (1999).

[29] A. Patrykiejew, S. Sokolowski, and D. Henderson, Mol. Phys. **95**, 211 (1998).

[30] T. Meistrer and D. Kroll, Phys. Rev. A **31**, 4055 (1985).

[31] R. D. Groot, Mol. Phys. **60**, 45 (1987).

[32] M. Calleja and G. Rickayzen, Mol. Phys. **79**, 809 (1993).

[33] P. Marsh, G. Rickayzen, and M. Calleja, Mol. Phys. **84**, 799 (1995).

[34] Y. Rosenfeld, Phys. Rev. Lett. **63**, 980 (1989).

[35] Y. Rosenfeld, Phys. Rev. A **42**, 5978 (1990).

[36] W. Bol, Mol. Phys. **45**, 605 (1982).

[37] Y. Rosenfeld, J. Phys.: Condens. Matter **8**, 9289 (1996).

[38] Y. Rosenfeld, J. Chem. Phys. **93**, 4305 (1990).

[39] Y. Rosenfeld, M. Schmidt, H. Lowen, and P. Tarazona, Phys. Rev. E **55**, 4245 (1997).

[40] P. Tarazona, Phys. Rev. Lett. **84**, 694 (2000).

[41] Y. Rosenfeld, J. Chem. Phys. **89**, 4272 (1988).

[42] C. J. Segura and W. G. Chapman, Mol. Phys. **86**, 415 (1995).